ChemComm

Tyrosine, cysteine, and proton coupled electron transfer in a ribonucleotide-inspired beta hairpin maquette

Journal:	*ChemComm*
Manuscript ID	CC-COM-05-2019-004067.R1
Article Type:	Communication

COMMUNICATION

Tyrosine, cysteine, and proton coupled electron transfer in a ribonucleotide reductase-inspired beta hairpin maquette

Received 00th January 20xx,
Accepted 00th January 20xx

DOI: 10.1039/x0xx00000x

Tyler G. McCaslin,[a,b] Cynthia V. Pagba,[a,b] Hyea Hwang,[c] James C. Gumbart,[a,b,d] San-Hui Chi,[a,e] Joseph W. Perry,[a,e] and Bridgette A. Barry[a,b]

Tyrosine residues act as intermediates in proton coupled electron transfer reactions (PCET) in proteins. For example, in ribonucleotide reductase (RNR), a tyrosyl radical oxidizes an active site cysteine via a 35-Å pathway that contains multiple aromatic groups. When singlet tyrosine is oxidized, the radical becomes a strong acid, and proton transfer reactions, which are coupled with the redox reaction, may be used to control reaction rate. Here, we characterize a tyrosine-containing beta hairpin, Peptide O, which has a cross-strand, noncovalent interaction between its single tyrosine, Y5, and a cysteine (C14). Circular dichroism provides evidence for a thermostable beta-turn. EPR spectroscopy shows that Peptide O forms a neutral tyrosyl radical after UV photolysis at 160 K. Molecular dynamics simulations support a phenolic/SH interaction in the tyrosine singlet and radical states. Differential pulse voltammetry exhibits pH dependence consistent with the formation of a neutral tyrosyl radical and a pK_a change in two other residues. A redox-coupled decrease in cysteine pK_a from 9 (singlet) to 6.9 (radical) is assigned. At pD 11, picosecond transient absorption spectroscopy after UV photolysis monitors tyrosyl radical recombination via electron transfer (ET). The ET rate in Peptide O is indistinguishable from the ET rates observed in peptides containing a histidine and a cyclohexylalanine (Cha) at position 14. However, at pD 9, the tyrosyl radical decays via PCET, and the decay rate is slowed, when compared to the histidine 14 variant. Notably, the decay rate is accelerated, when compared to the Cha 14 variant. We conclude that redox coupling between tyrosine and cysteine can act as a PCET control mechanism in proteins.

Proton coupled electron transfer (PCET) involving the tyrosine aromatic ring is fundamental to important biological processes, including photosynthesis and DNA synthesis. In DNA synthesis, the enzyme, ribonucleotide reductase (RNR), combines proton transfer with a long distance radical transfer reaction.[5] This reaction occurs over 35 Å using a radical initiator, Y122 (beta) and three other tyrosine residues, which function as intermediates. The radical transfer pathway spans the interface between two RNR subunits, alpha and beta.[5] Oxidation of the tyrosine aromatic ring is coupled with proton transfer because oxidation dramatically decreases the pK_a of the phenolic OH group.[6] PCET occurs at pH values below the pK_a of tyrosine; an electron transfer (ET) reaction occurs above the pK_a.

The use of peptide mimics or maquettes allows the mechanism of PCET reactions to be investigated in detail. The usefulness of modeling in structurally tractable beta hairpins has been demonstrated.[1, 7-13] Previously, a peptide, Peptide A (Figure 1A), which carries out a PCET reaction between tyrosine and histidine, was synthesized. The NMR structure of Peptide A (Figure 1A) reveals a cross strand, pi-pi interaction between the single tyrosine, Y5, and histidine (H14). However, the tyrosine and histidine are not directly hydrogen bonded in the lowest energy structure. When tyrosine is oxidized in Peptide A, either photochemically or electrochemically, the cross strand histidine undergoes a coupled pK_a shift. Protonation of histidine will occur in the mid-pH range. This pK_a shift leads to so called redox coupling, in which the oxidation reaction alters proton affinity and a change in proton affinity in turn alters the driving force of the reaction. This pK_a shift is detectable as inflection points in a plot of peak potential versus pH. Mutagenesis of histidine to Cha eliminated the inflection points assigned to the imidazole side chain in Peptide A. Interestingly, the rate of tyrosyl radical recombination was slowed when the histidine was changed to Cha in a second peptide, Peptide C (Figure 1B). [1, 7-13]

[a] School of Chemistry and Biochemistry, Georgia Institute of Technology, Atlanta, GA 30332, U. S. A.
[b] The Parker H. Petit Institute of Bioengineering and Bioscience, Georgia Institute of Technology, Atlanta, GA 30332, U. S. A.
[c] School of Materials Science and Engineering, Georgia Institute of Technology, Atlanta, GA 30332, U. S. A.
[d] School of Physics, Georgia Institute of Technology, Atlanta, GA 30332, U. S. A.
[e] Center of Organic Photonics and Electronics, Georgia Institute of Technology, Atlanta, GA 30332, U. S. A.
*Corresponding author, bridgette.barry@chemistry.gatech.edu
Electronic Supplementary Information (ESI) available: Supporting material includes materials and methods, tables of charge states and biexponential fits, CD data, MD simulations, TRAS spectra and kinetics with exponential fits and residuals. See DOI: 10.1039/x0xx00000x

Here, we test whether such functionally relevant redox coupling occurs in another peptide, Peptide O. Peptide O contains a SH/tyrosine interacting pair (Figure 1C). Figure S1A presents circular dichroism (CD) data acquired from Peptide O. The beta turn makes a major contribution to the CD. The CD

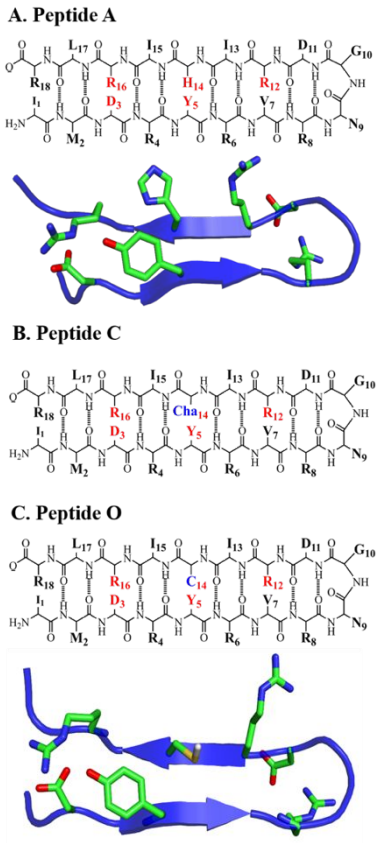

Figure 1. Primary sequences and structures of Peptide A (A), Peptide C (B), and Peptide O (C). The structure of Peptide A (A) was determined by NMR and reported previously.[1] The structure of Peptide O was modeled using PEP-FOLD[2-4] and molecular replacement based on the NMR structure of Peptide A.

data show negative ellipticity at 198 nm (solid). Heating to 80°C causes a loss of this negative ellipticity (dot-dashed line); this effect is reversible when the sample is cooled to 20°C (dashed). As observed in Figure S1B, the CD signature of Peptide O is similar to the signal derived from Peptide A. Further, the CD spectra of Peptide O, which contains a single cysteine, were independent of the addition of the reductant, dithiothreitol (DTT) (Figure S2). This result suggests that Peptide O does not form intermolecular disulfide linkages under these conditions.

Titration of pH allows access to different charge states of the Y5 and C14 side chains in Peptide O (Figure S3A and B). As illustrated in Figure S3C, UV photolysis at pH 9 produces a neutral tyrosyl radical. Figure S4D presents the EPR spectrum of Peptide O after UV photolysis at 160 K. The g=2.004 signal is characteristic of neutral tyrosyl radical.[6, 14] This signal arises from hyperfine couplings to the 3,5 ring and the methylene hydrogens. The EPR lineshape is sensitive both to spin density distribution and conformation.[6] Previous electrostatic calculations have shown that there is a rearrangement of charge when tyrosine/tyrosinate are compared to the radical.[15] This Peptide O signal is similar to the EPR spectrum observed in tyrosine (Figure S4A) and reported previously from Peptide A.[1] The g = 2.004 signal is not observed after photolysis of cysteine (Figure S4B) but is observed, with a similar lineshape in an equimolar mixture of tyrosine and cysteine (Figure S4C).

To investigate the structural stability of Peptide O, MD simulations were employed.[8] The stability of the β-hairpin conformation was examined for three independent 200-ns long MD simulations each. The Supporting Information (Figure S5) presents plots of secondary structure vs. time for Peptide O in various charge states (Table S1 and Figure S3A). In all the simulations, the amino and carboxyl termini are blocked and uncharged.

The per-residue secondary structure assignment as a function of time was examined over the entire simulation (Figure S5). Peptide O YH-C (both tyrosine and cysteine protonated, Table S1) retained its β-hairpin structure over the simulation period, i.e., the secondary structure of residues 4−7 and 12−15 exhibited no change in two out of three runs (Figure S5). While the second run produced a less stable β-hairpin structure compared to the other two runs, the peptide never lost its hairpin structure but instead developed a longer β-turn in the middle. We conclude that Peptide O YH-C is stable over time and never reaches the unfolded state in all simulation runs. When the cysteine is deprotonated, Peptide O YH-deC, only one of three runs exhibits stable behavior. Moreover, the peptide lost secondary structure for half of one simulation (second run) and immediately became unfolded in another (third run) as shown in Figure S5.

We hypothesized that the stability of Peptide O YH-C is a result of the S−H/π interaction[16-18] between Y5 and C14. We measured the distance between the center of mass of aromatic carbons (Y5) and the thiol H (C14), i.e., that for an S-H/π interaction (Figure 2). Our results show that 41% of the time, the H from the thiol functional group of C14 is located near (within 2.2-3.9 Angstrom) the center of the aromatic ring. This interaction maximizes favorable electrostatic interactions with all electrons of the π system (Figure 2A). Consistent with this hypothesis, when cysteine is deprotonated (Figure 2B), resulting in a loss of this noncovalent interaction, the peptide's β-hairpin structure became unstable in most runs, as exhibited in secondary structure assignment (Figure S5). As shown in Figure 2B, formation of the tyrosyl radical is predicted to increase the average distance between the aromatic ring and the thiol group. Loss of negative charge from the ring due to radical formation may promote deprotonation of the cysteine.

Because the MD simulations provided evidence of an interaction between Y5 and C14, a pH titration was performed to measure the tyrosine pK_a (Figure S6A). The results in Figure S6A show that the tyrosine pK_a is 9.7 and indistinguishable from Peptide A.

The peak potential was measured as a function of pH in Peptide O, and the results were distinct compared to previous results acquired Peptide A (Figure S6B). While the oxidation of tyrosine is not reversible, a detailed analysis has shown that the correction factor is small under the conditions used here.[1, 7, 19] Note that the Peptide O data are distinct from data acquired from Peptide A (Figure S6B, orange) and the prediction for tyrosine solution (Figure S6C, dashed). The plot of Peptide O potential versus pH exhibits additional inflection point and

requires a modified Nernst equation. For example, a function that reflects pK_a shifts in three amino acid residues was used to represent the data (Figure S6C and legend). The pK_a values are evident as positive and negative inflection (Figure S6B and C) points, corresponding to proton transfer reactions in the radical and singlet states. For example, the pK_a of the tyrosine is an inflection point at 9.7; the pK_a of the tyrosyl radical state is below zero and is not in the data set. Of the other inflection points observed in Peptide O, the pK_a of ~ 9 is assignable to cysteine in the singlet state, and the pK_a of ~6.9 is assignable to cysteine in the radical state (Figure S6B and C, solid). A pK_a shift in an additional amino acid residue, which may be aspartate, is also evident at pH 6. A pK_a shift in an aspartate residue was also reported in Peptide A.[1,9] The Peptide O results support the conclusion that C14 undergoes a redox-linked shift in proton affinity when Y5 is oxidized. This change in proton affinity will result in deprotonation of the thiol group in the mid pH range. In contrast, in Peptide A, oxidation of tyrosine led to a shift in histidine pK_a from 6.0 (singlet) to 9 (radical) and to protonation of the histidine side chain.

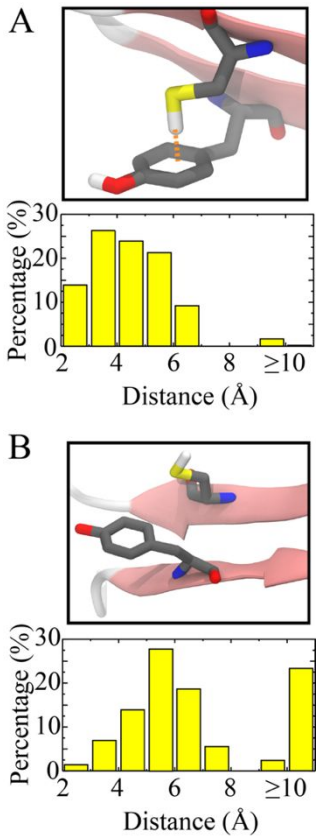

Figure 2. Simulation results from Peptide O. In both parts, the top image is a snapshot of Y5 and C14, and the bottom is the distribution of distances between the thiol H and the aromatic carbons (center of mass of CA atoms) from 3 runs of 200 ns each. (A) Peptide O YH-C with the S-H/π interaction indicated (occurs 41% of the time). (B) Radical Peptide O Y•-C, which mostly lacks the S-H/π interaction (8%).

To assess the kinetic consequences of redox coupling between C14 and Y5 in Peptide O, the recombination of tyrosyl radical was measured on the picosecond time scale. The tyrosyl radical was generated using 280 nm photolysis. Due to the limited solubility of Peptide O in H_2O buffers, D_2O buffers were employed. In previous work,[11, 12] changing H14 to Cha in Peptide C decreased the rate at which Y5 recombines with the solvated electron and a proton at pH 9 (via PCET, Figure S3D). This was attributed to a change in solvent reorganization energy. Notably, there was no significant alteration observed at pH 11, which supports electron transfer (ET, Figure S3E).

Figures S7D presents TRAS of Peptide O af pD 11. The spectra of Peptide O (Figure S7D) are similar to tyrosinate, Peptide A, and Peptide C at pD 11 (Figure S7A-C and refs.[11, 12]). The decay of the tyrosyl radical at 410 nm was monitored. The kinetic analysis (Figure 3B and Figure S9D-F) shows that Peptide A, C, and O have similar ET decay kinetics (Table S2). The decay rates in the three peptides are accelerated relative to tyrosinate. Note that the decay rates of the solvated electron (650 nm) and S1 excited state (520 nm) are also similar in all three peptides (Table S2).

TRAS were also recorded at an apparent pD of 9 from Peptide O (Figure S8D). At this pD, the phenolic group of tyrosine is in the OD form. Therefore, the reaction observed after UV photolysis corresponds to radical recombination with the solvated electron and a deuteron (Figure S3D). The spectra acquired from tyrosine, Peptide A, C, and O are similar (Figure S8A-D). However, the three peptides exhibit distinct radical decay kinetics when compared to each other (Figure 3A and S9A-C). In particular, the fast phase in Peptide O is a factor of ten slower in rate when compared to Peptide A, which contains a histidine at position 14 (Table S2). Notably, the decay kinetics were faster when compared to Peptide C, containing Cha at position 14 (Table S2). These data support the conclusion that deprotonation of cysteine promotes the PCET reaction, relative to the hydrophobic Cha functional group.

To summarize the recombination reaction in Peptide O at pD 9, an electron is transferred to the radical, the S- group partially protonates due to its pK_a shift from 6.9 (radical) to 9, and a proton/deuteron is transferred to the tyrosyl radical. The order of these steps defines the mechanism of PCET. In principle, the reaction may occur proton transfer first (PTET, producing a cation radical intermediate), electron transfer first (ETPT, producing a tyrosinate intermediate), or a coupled CPET mechanism. A PTET mechanism would form the highly unstable cation radical, which has a unique visible band[20] and is not observed here. Therefore, we conclude that the recombination reaction occurs through an ETPT or a CPET mechanism, as previously suggested for Peptide A.[13,14]

MD simulations and UV resonance Raman spectroscopy have provided evidence for a secondary structure change when tyrosine is oxidized in some of the beta hairpin peptides.[10] Two charge states, containing tyrosine or tyrosinate in Peptide A, were deduced to be stable on the hundreds of nanoseconds time scale. On the other hand, tyrosyl radical containing Peptide A unfolded in the simulations after 50 ns. Peptide C was unstable after 50 ns in both the tyrosinate and the tyrosyl-radical containing forms. Note that the CD spectrum provides evidence for a thermostable turn in all the peptides.[10]

On the 2-ns time scale employed for TRAS, these changes in hydrogen bonding and secondary structure are not expected to play a role. On longer time scales, at pD 11, the MD simulations

predict that Peptide O unfolds due to the presence of the tyrosinate side chain. At pD 9, where tyrosine is the predominant charge state, contributions from unfolded states are likely to be insignificant.

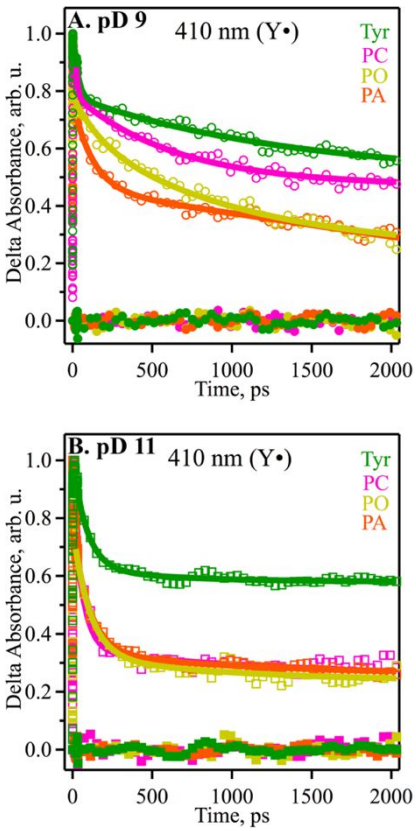

Figure 3. Kinetics of tyrosyl radical decay as derived from TRAS on tyrosine/tyrosinate and peptides in pD 9 (A) and pD 11 (B) buffers. Data were recorded after 280-nm photolysis. Samples were tyrosine/tyrosinate (green), Peptide A (orange), Peptide C (pink) and Peptide O (yellow). In each sample, the absorption of the neutral tyrosyl radical was monitored at 410 nm. Double exponential fits (starting from 20 ps) are superimposed as the solid lines, and the closed circles/squares are the corresponding residuals. Fitting parameters are presented in Table S2. The data were averaged from at least two independent measurements. The analyte concentration, 1 mM; buffer, 5 mM borate-NaOD.

In summary, we describe a model system in which a cysteine undergoes a pK_a shift and a deprotonation reaction when a tyrosine residue is oxidized. This interaction has a significant effect on the stability of the tyrosyl radical and small effects on the driving force for the reaction. In class 1a RNR, an essential cysteine in the substrate binding site is oxidized by tyrosine. Y122 beta is the radical initiator; the radical transfer pathway contains Y356 in beta and Y730 and 731 in the alpha subunit. Y731 is the proximate oxidant for C439. The distance between Y731 and the cysteine is 3.4 Angstrom. The overall reaction, in which tyrosine oxidizes cysteine, is predicted to be slightly uphill in energy. [21] Extrapolating from this Peptide O model, transient oxidation of Y731 may trigger a decrease in the pK_a of C439. This is of interest because a thiolate side chain is more readily oxidized, compared to a thiol. Peptide O provides an example in which through space, noncovalent interactions between tyrosine and cysteine alter radical stability.

Conflicts of interest

There are no conflicts to declare.

Notes and references

Supported by NSF CLP 18-01926 (B.A.B.) and NSF MCB 1452464 (J.C.G.).

1. R. Sibert, M. Josowicz, F. Porcelli, G. Veglia, K. Range and B. A. Barry, *J. Am. Chem. Soc.*, 2007, **129**, 4393-4400.
2. J. Maupetit, P. Derreumaux and P. Tuffery, *Nucleic Acids Res.*, 2009, **37**, W498-503.
3. J. Maupetit, P. Derreumaux and P. Tufféry, *J. Comput. Chem.*, 2010, **31**, 726-738.
4. P. Thévenet, Y. Shen, J. Maupetit, F. Guyon, P. Derreumaux and P. Tufféry, *Nucleic Acids Res.*, 2012, **40**, W288-W293.
5. E. C. Minnihan, D. G. Nocera and J. Stubbe, *Acc. Chem. Res.*, 2013, **46**, 2524-2535.
6. B. A. Barry, M. K. El-Deeb, P. O. Sandusky and G. T. Babcock, *J. Biol. Chem.*, 1990, **265**, 20139-20143.
7. R. S. Sibert, M. Josowicz and B. A. Barry, *ACS Chem. Biol.*, 2010, **5**, 1157-1168.
8. H. Hwang, T. G. McCaslin, A. Hazel, C. V. Pagba, C. M. Nevin, A. Pavlova, B. A. Barry and J. C. Gumbart, *J. Phys. Chem. B*, 2017, **121**, 3536-3545.
9. T. G. McCaslin, C. V. Pagba, S.-H. Chi, H. J. Hwang, J. C. Gumbart, J. W. Perry, C. Olivieri, F. Porcelli, G. Veglia, Z. Guo, M. McDaniel and B. A. Barry, *J. Phys. Chem. B*, 2019, **123**, 2780-2791.
10. C. V. Pagba and B. A. Barry, *J. Phys. Chem. B*, 2012, **116**, 10590-10599.
11. C. V. Pagba, S. H. Chi, J. Perry and B. A. Barry, *J. Phys. Chem. B*, 2015, **119**, 2726-2736.
12. C. V. Pagba, T. G. McCaslin, S. H. Chi, J. W. Perry and B. A. Barry, *J. Phys. Chem. B*, 2016, **120**, 1259-1272.
13. C. V. Pagba, T. G. McCaslin, G. Veglia, F. Porcelli, J. Yohannan, Z. Guo, M. McDaniel and B. A. Barry, *Nat. Commun.*, 2015, **6**, 10010.
14. B. A. Barry and G. T. Babcock, *Proc. Nat. Acad. Sci. USA*, 1987, **84**, 7099-7103.
15. K. Range, I. Ayala, D. York and B. A. Barry, *J. Phys. Chem. B*, 2006, **110**, 10970-10981.
16. H. S. Biswal and S. Wategaonkar, *J. Phys. Chem. A*, 2009, **113**, 12774-12782.
17. A. L. Ringer, A. Senenko and C. D. Sherrill, *Protein Sci.*, 2007, **16**, 2216-2223.
18. C. R. Forbes, S. K. Sinha, H. K. Ganguly, S. Bai, G. P. A. Yap, S. Patel and N. J. Zondlo, *J. Am. Chem. Soc.*, 2017, **139**, 1842-1855.
19. A. Harriman, *J. Phys. Chem.*, 1987, **91**, 6102-6104.
20. T. A. Oliver, Y. Zhang, A. Roy, M. N. Ashfold and S. E. Bradforth, *J. Phys. Chem. Lett.*, 2015, **6**, 4159-4164.
21. B. L. Greene, J. Stubbe and D. G. Nocera, *J. Am. Chem. Soc.*, 2018, **140**, 15744-15752.